Studies of granularity of a hadronic calorimeter for tens-of-TeV jets at a 100 TeV *pp* collider

S.V. Chekanov[a], A.V. Kotwal[b,c], J. Proudfoot[a], S. Sen[b], N.V. Tran[c], S.-S. Yu[e], Chih-Hsiang Yeh[e]

[a] *HEP Division, Argonne National Laboratory, 9700 S. Cass Avenue, Argonne, IL 60439, USA.*
[b] *Department of Physics, Duke University, USA*
[c] *Fermi National Accelerator Laboratory*
[d] *Department of Physics, Michigan State University, 220 Trowbridge Road, East Lansing, MI 48824*
[e] *Department of Physics, National Central University, Chung-Li, Taoyuan City 32001, Taiwan*

Abstract

Texts

Keywords: multi-TeV physics, *pp* collider, future hadron colliders, FCC, SppC

1. Introduction

Particle collisions at energies beyond those attained at the LHC will lead to many challenges for detector technologies. Future experiments, such as high-energy LHC (HE-LHC), future circular *pp* colliders of the European initiative, FCC-hh [**?**] and the Chinese initiative, SppC [**?**] will be required to measure high-momentum bosons (W, Z, H) and top quarks with strongly collimated decay products that form jets. Studies of jet substructure can help identify such particles.

The reconstruction of jet substructure variables for collimated jets with transverse momentum above 10 TeV require an appropriate detector design. The most important for reconstruction of such jets are tracking and calorimeter. Recently, a number of studies [**?** **?** **?**] have been discussed using various fast simulation tools, such as Delphes [**?**], in which momenta of particles are smeared to mimic detector response.

A major step towards the usage of full Geant4 simulation to verify the granularity requirements for calorimeters was made in [**?**]. The studies included in this paper have illustrated a significant impact of granularity of electromagnetic (ECAL) and hadronic (HCAL) calorimeters on the shape of hadronic showers calculated using calorimeter hits for two particles separated by some angle. It was concluded that high granularity is essential in resolving two close-by particles for energies above 100 GeV.

This paper makes another step in understanding understanding of this problem in terms of high-level physics quantities typically used in physics analyses. Similar to the studies presented in [**?**], this paper is based on full Geant4 simulation with realistic jet reconstruction.

Email addresses: chekanov@anl.gov (S.V. Chekanov), ashutosh.kotwal@duke.edu (A.V. Kotwal), proudfoot@anl.gov (J. Proudfoot), sourav.sen@duke.edu (S. Sen), ntran@fnal.gov (N.V. Tran), syu@cern.ch (S.-S. Yu), jwzuzelski18@gmail.com (Chih-Hsiang Yeh)

Preprints: XXX-XXX *January 19, 2018*

2. Simulation of detector response and event reconstruction

The description of the detector and software used for this paper is discussed in [**?**]. We use the SiFCC detector geometry with a software package that represents a versatile environment for simulations of detector performance, testing new technology options, event reconstruction techniques for future 100 TeV colliders. The event samples used in this paper are available from the HepSim database [**?**].

The GEANT4 (version 10.3) [**?**] simulation of calorimeter response was complimented with full reconstruction of calorimeter clusters using the Pandora algorithm [**?** **?**]. Calorimeter clusters were built from calorimeter hits in the ECAL and HCAL after applying the corresponding sampling fractions. No other corrections are applied. Hadronic jets were reconstructed with the FASTJET package [**?**] using the anti-k_T algorithm [**?**] with a distance parameter of 0.5.

3. Studies of effective jet radius

The effective radius is the average of the energy weighted radial distance in $\eta - \phi$ space of jet constituents. Recently, it has been studied for multi-TeV jets in Ref.[**?**].

New we sill study jet splitting the effect of granularity on jet splitting scales. A jet k_T splitting scale [**?**] is defined as a distance measure used to form jets by the k_T recombination algorithm [**?** **?**]. This has been studied by ATLAS [**?**], and more recently in the context of 100 TeV physics [**?**]. The distribution of the splitting scale $\sqrt{d_{12}} = \min(p_T^1, p_T^2) \times \delta R_{12}$ [**?**] at the final stage of the k_T clustering, where two subjets are merged into the final one, is shown in Fig. 2.

4. Studies of signal and background separation using calorimeter clusters

In this section, we study different jet substructure variables and compare their ability to separate the signal and the background for different detector sizes using calorimeter clusters.

Figures 3–5 show the ROC curves of three variables, $c_2^{(1)}$ [**?**] , τ_{21} [**?**], and τ_{32} [**?**], respectively. Three different cell sizes of the HCAL are compared for four collision energies. For different cell sizes with the same signal efficiency, the one with the highest background rejection rate, namely (1-background efficiency), has the highest separate power.

In Figure 3 for the variable $c_2^{(1)}$, the ROC curves of the three detector cell sizes are close to each other for each collision energy. Therefore, this variable is not sensitive to the detector cell size.

For the τ_{21} variable in Figure 4, at 5 TeV, the smallest detector size (1×1 cm) can separate the background from the signal well. However, this is not the usual case as the ROC curves nearly merge together at higher collision energy. In addition, the detector with the bigger size tends to have higher separation power than the smaller detector size in 20 and 40 TeV collision energy.

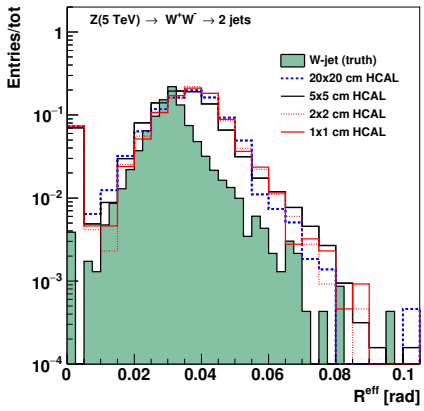

(a) 5 TeV

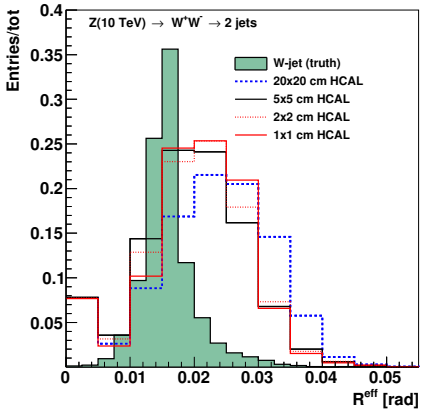

(b) 10 TeV

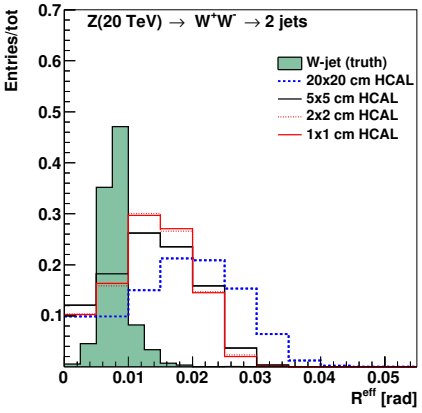

(c) 20 TeV

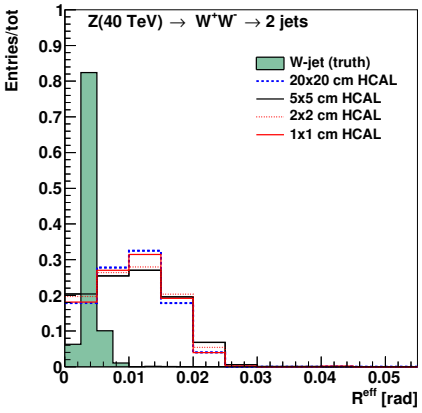

(d) 40 TeV

Figure 1: Jet effective radius for different jet transverse moment and HCAL granularity.

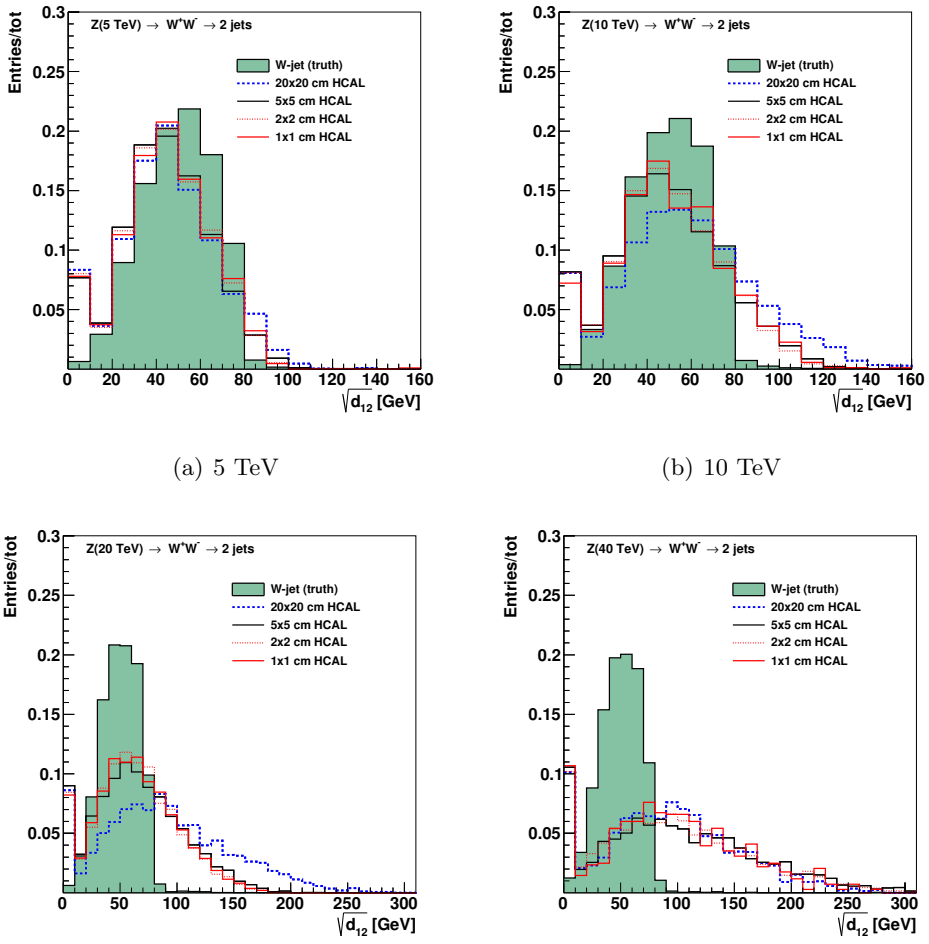

(a) 5 TeV

(b) 10 TeV

(c) 20 TeV

(d) 40 TeV

Figure 2: Jet splitting scale for different jet transverse moment and HCAL granularity.

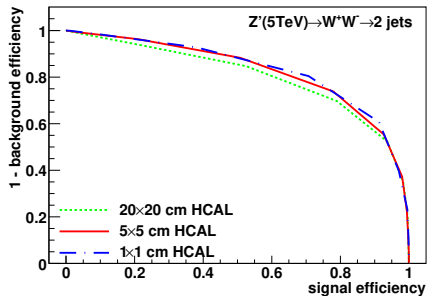

(a) 5 TeV

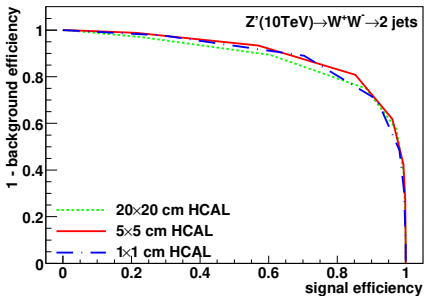

(b) 10 TeV

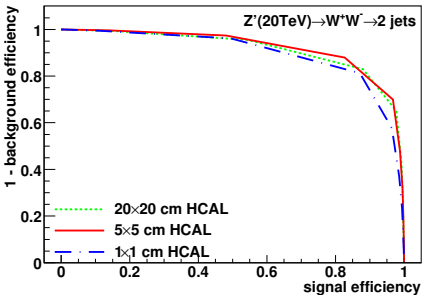

(c) 20 TeV

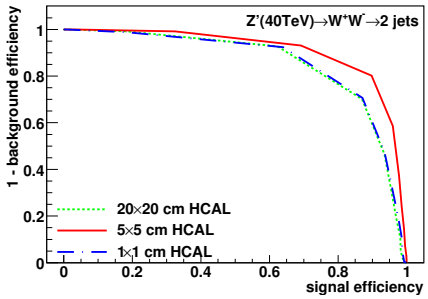

(d) 40 TeV

Figure 3: Signal efficiency versus background rejection rate using $c_2^{(1)}$.The energies of collision at (a)5, (b)10, (c)20, (d)40TeV are shown here. In each picture, the three ROC curves correspond to different detector sizes.

Figure 5 shows the variable τ_{32}, where the smallest detector size has the best separation power for all collision energies.

In conclusion, in all the cases of energy and detector size, the variable $c_2^{(1)}$ has the best separation power compared to the other two variables. In addition, the variable τ_{32} follows the expectation that smaller detector size has better separation power.

5. Studies of signal and background separation using Mann-Whitney U test

In this section, we study different jet substructure variables and compare their ability to separate the signal and background for different detector cell sizes using the Mann-Whitney U test.

By the definition of the Mann-Whitney U test, if the value of U is close to 0.5, it means that the signal and background distributions have almost identical shapes, i.e. the separation power of the variable is bad. On the other hand, if the U value is close to 0, it means that the distributions of the signal and the background are very different

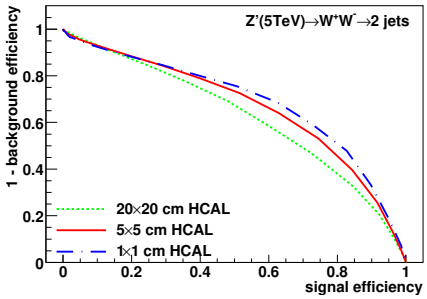

(a) 5 TeV

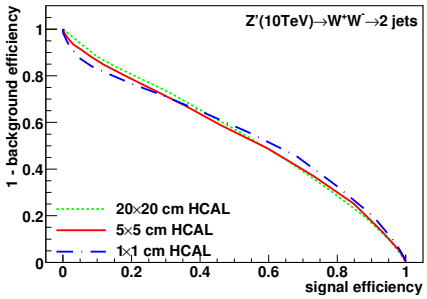

(b) 10 TeV

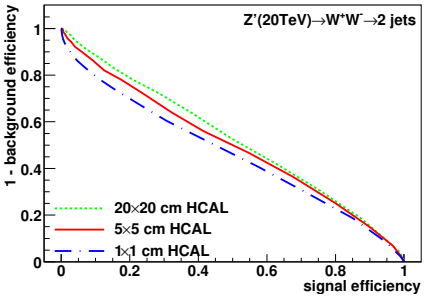

(c) 20 TeV

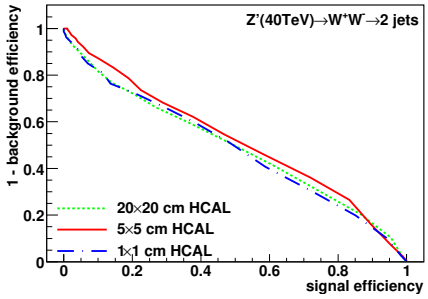

(d) 40 TeV

Figure 4: Signal efficiency versus background rejection rate using τ_{21}.The energies of collision at (a)5, (b)10, (c)20, (d)40TeV are shown here. In each picture, the three ROC curves correspond to different detector sizes.

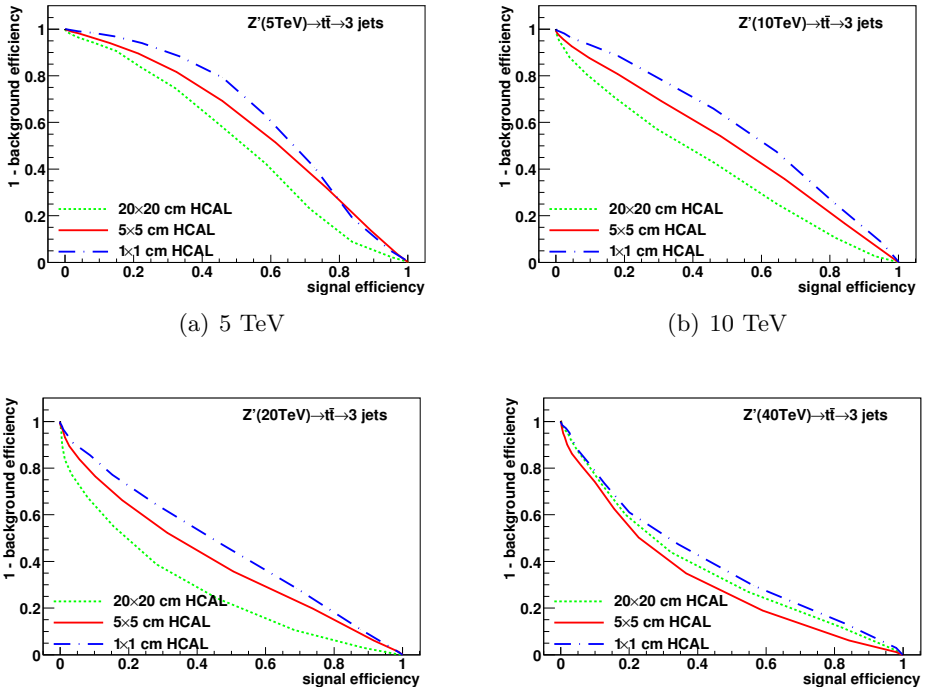

(a) 5 TeV (b) 10 TeV

(c) 20 TeV (d) 40 TeV

Figure 5: Signal efficiency versus background rejection rate using τ_{32}.The energies of collision at (a)5, (b)10, (c)20, (d)40TeV are shown here. In each picture, the three ROC curves correspond to different detector sizes.

from each other and the separation power of the variable is great.

Figure 6 shows the representative sample of the distributions for τ_{21},τ_{32}, in different detector sizes with their corresponding U value. In τ_{21}, the separation power is better when the detector size is smaller. However, the separation power of tau32 does not improve when the detector size gets smaller.

Figure 7 shows the summary plots of the clustering in Mann-Whitney U test for the three different variables. In τ_{21}, 5 TeV has the better separation power when the detector size is smaller. However, there is not much improvement in higher energy collisions. In τ_{32}, 5 TeV has also better separation power on smaller detector size but higher energy collisions seem to have better separation power when the detector size is bigger. The $c_2^{(1)}$ does not seem to have any significant improvement in its separation power as the detector size gets smaller for all energy collision. Nevertheless, the U values of the $c_2^{(1)}$ are better than theτ_{21} and τ_{32}. In conclusion, the $c_2^{(1)}$ variable is the best parameter as its separation power is better than the other variable and does not have a significant improvement in higher energy collision.

Figure 8 shows the summary plots of the rawhit cut at 0.5 GeV in Mann Whitney U test for the three different variables. In τ_{21}, 5 and 10 TeV have better separation power on smaller detector sizes. However, there is no significant improvement in the separation power of higher energy collisions. The τ_{32} does not have any significant improvement in its separation power as the detector size gets smaller for all energy collision. Lastly, there is a slight improvement in separation power for 5, 10, and 20 TeV energy collision in $c_2^{(1)}$. At 40 TeV, no significant improvement is observed. In conclusion, the $c_2^{(1)}$ variable is the best parameter as it has the best separation power at 40 TeV energy collision than the other variables.

Acknowledgements

This research was performed using resources provided by the Open Science Grid, which is supported by the National Science Foundation and the U.S. Department of Energy's Office of Science. We gratefully acknowledge the computing resources provided on Blues, a high-performance computing cluster operated by the Laboratory Computing Resource Center at Argonne National Laboratory. Argonne National Laboratory's work was supported by the U.S. Department of Energy, Office of Science under contract DE-AC02-06CH11357. The Fermi National Accelerator Laboratory (Fermilab) is operated by Fermi Research Alliance, LLC under Contract No. DE-AC02-07CH11359 with the United States Department of Energy.

Appendix

Another study about the c variables

In the past paper [**?**], It mention that in some process at c_2, when $\beta = 1.7$, it will have the best separation power. We try to use this in our study to see whether it is

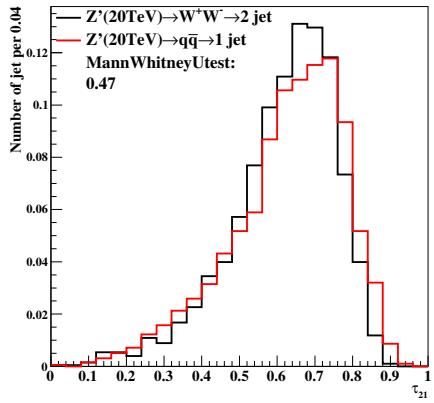

(a) 20×20(cm×cm)

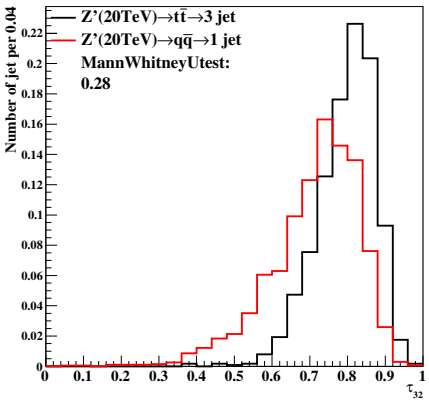

(b) 20×20(cm×cm)

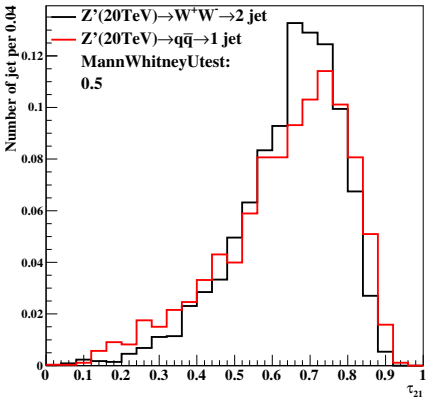

(c) 5×5(cm×cm)

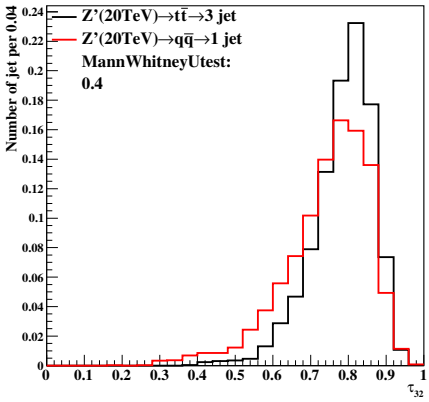

(d) 5×5(cm×cm)

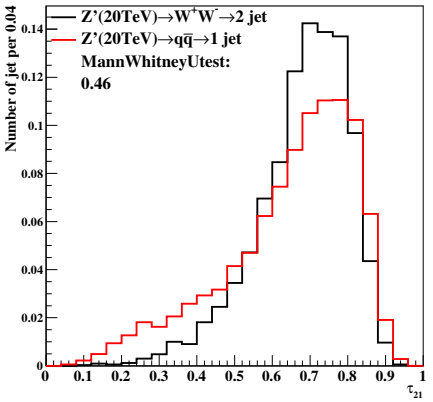

(e) 1×1(cm×cm)

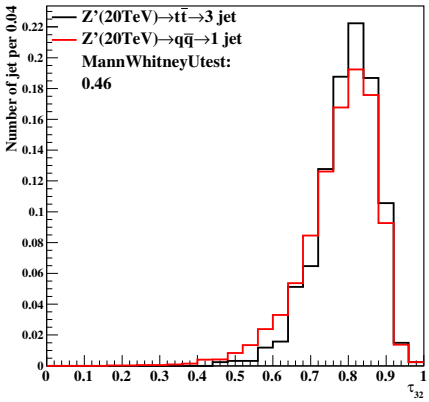

(f) 1×1(cm×cm)

Figure 6: Distributions and U value in 20TeV energy collision for τ_{21},τ_{32} in different detector sizes. Cell Size in 20×20,5×5 and 1×1(cm×cm) are shown here.

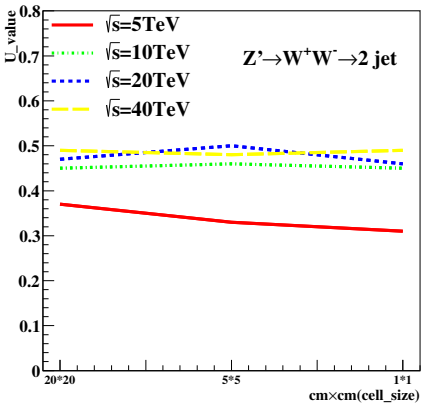

(a) τ_{21}

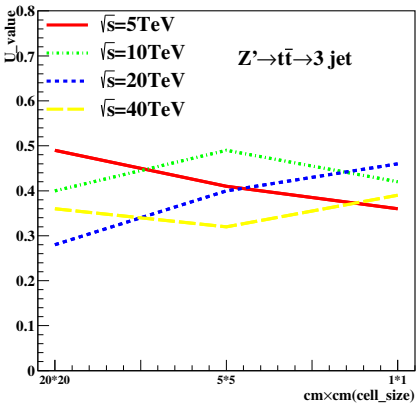

(b) τ_{32}

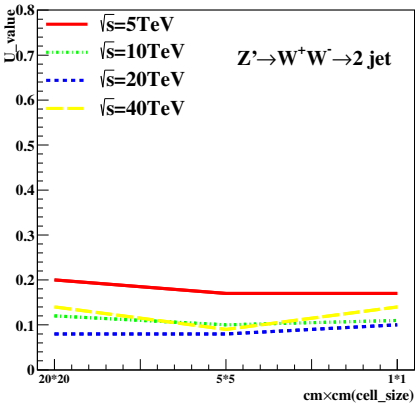

(c) $c_2^{(1)}$

Figure 7: U value for τ_{21},τ_{32} and $c_2^{(1)}$ at different collision energies correspond to different detector sizes in cluster. The energies of collision at 5, 10, 20, 40TeV are shown in each picture.

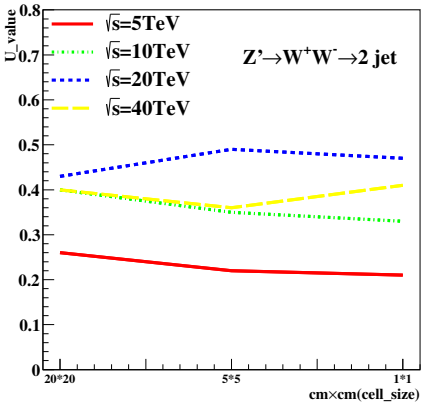

(a) τ_{21}

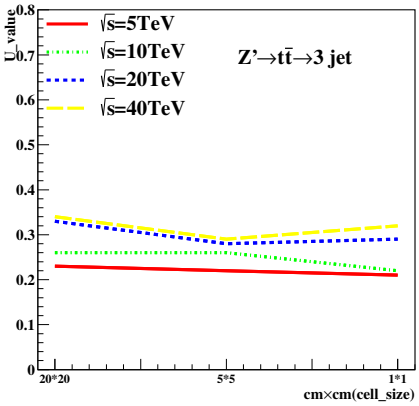

(b) τ_{32}

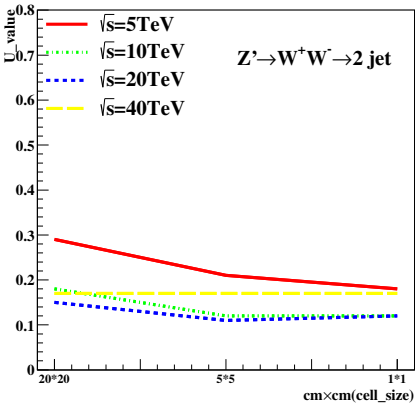

(c) $c_2^{(1)}$

Figure 8: U value for τ_{21},τ_{32} and $c_2^{(1)}$ at different collision energies correspond to different detector sizes in rawhit cut at 0.5GeV. The energies of collision at 5, 10, 20, 40TeV are shown in each picture.

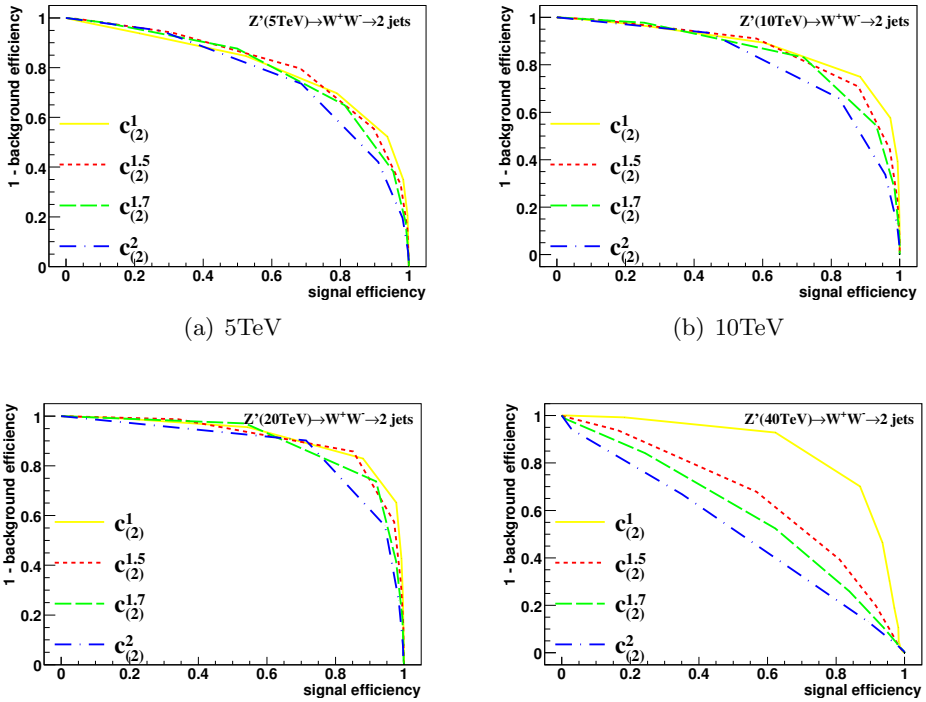

(a) 5TeV (b) 10TeV

(c) 20TeV (d) 40TeV

Figure 9: Signal efficiency versus background rejection rate using $c_2^{(1)}$,$c_2^{(1.5)}$,$c_2^{(1.7)}$,$c_2^{(2)}$ in different energies of collision at 20×20(cm×cm) cell size.The energies of collision at (a)5, (b)10, (c)20, (d)40TeV are shown here.

suitable for our research.

In Figure 9,10 and 11, they are the ROC curves of the different β quantities in c_2 at different energies of collision. We can see that in all cell sizes, separation power isn't improved by increasing β quantity to 1.7. We can see from $\beta = 1$ to $\beta = 2$, the separation power is worse and worse in all cell sizes in all energies of collision.

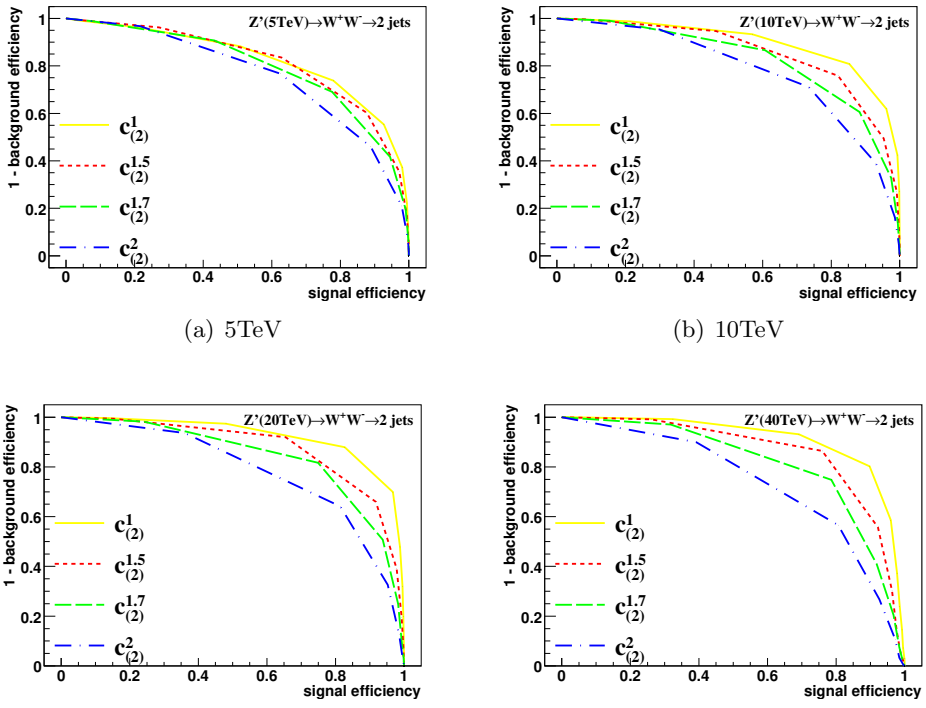

(a) 5TeV (b) 10TeV

(c) 20TeV (d) 40TeV

Figure 10: Signal efficiency versus background rejection rate using $c_2^{(1)}$,$c_2^{(1.5)}$,$c_2^{(1.7)}$,$c_2^{(2)}$ in different energies of collision at 5×5(cm×cm) cell size.The energies of collision at (a)5, (b)10, (c)20, (d)40TeV are shown here.

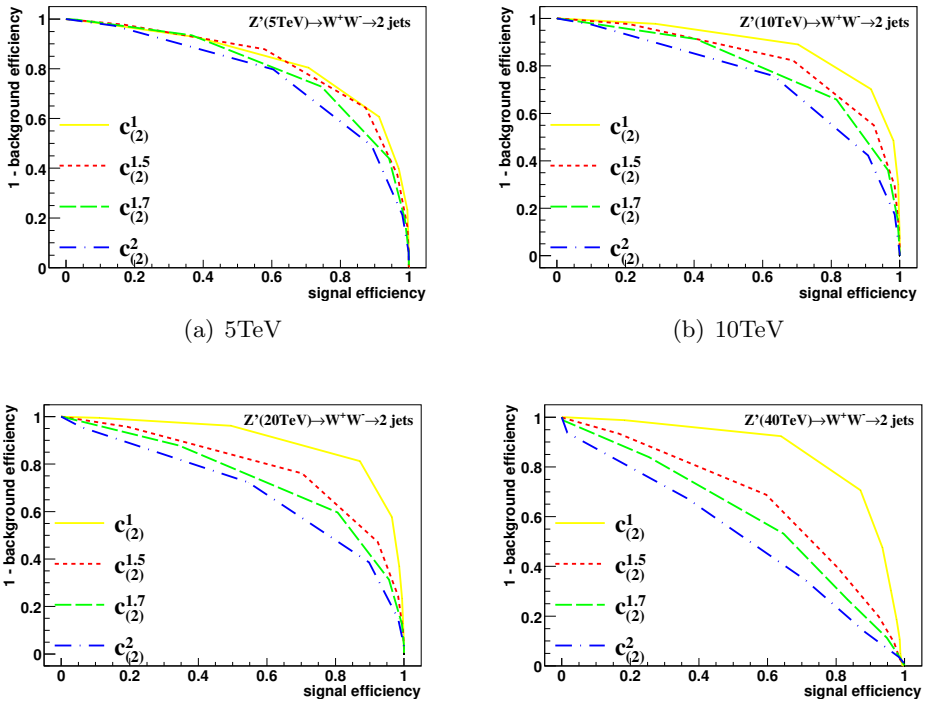

(a) 5TeV (b) 10TeV

(c) 20TeV (d) 40TeV

Figure 11: Signal efficiency versus background rejection rate using $c_2^{(1)}$,$c_2^{(1.5)}$,$c_2^{(1.7)}$,$c_2^{(2)}$ in different energies of collision at 1×1(cm×cm) cell size.The energies of collision at (a)5, (b)10, (c)20, (d)40TeV are shown here.

References